NASA TECHNICAL MEMORANDUM

NASA TM X-52238

NASA TM X-52238

SHADOW SHIELD EXPERIMENTAL STUDIES

by R. H. Knoll, E. R. Bartoo,
and R. J. Boyle
Lewis Research Center
Cleveland, Ohio

TECHNICAL PAPER proposed for presentation at Conference on Long-Term Cryo-Propellant Storage in Space sponsored by the National Aeronautics and Space Administration
Huntsville, Alabama, October 12-13, 1966

NATIONAL AERONAUTICS AND SPACE ADMINISTRATION · WASHINGTON, D.C. · 1966

SHADOW SHIELD EXPERIMENTAL STUDIES

by R. H. Knoll, E. R. Bartoo, and R. J. Boyle

Lewis Research Center
Cleveland, Ohio

TECHNICAL PAPER proposed for presentation at

Conference on Long-Term Cryo-Propellant Storage in Space
sponsored by the National Aeronautics and Space Administration
Huntsville, Alabama, October 12-13, 1966

NATIONAL AERONAUTICS AND SPACE ADMINISTRATION

ABSTRACT

Experiments were performed on multiple flat-plate shadow shields to determine the effect of shield spacing, number, emissivity, and lateral conduction on thermal performance. In general, the analytical results closely agreed with experimental data. Analytical results for targeted shields (coated annular rings) demonstrated a method of shield temperature control and were in close agreement with experimental data. Tests on a complete shadow-shield system demonstrated the interaction between shields and their supporting structure and how strut heat leaks could be reduced. The use of a ring with a shield material stretched across one or both sides provided a lightweight highly efficient shield.

E-3628

SYMBOLS

k	thermal conductivity, Btu/(hr)(ft)(^{o}R)
L	distance between heat source and heat sink, in.
R	radial distance from center of shield, in.
R_o	radius of shields, heat source and heat sink, in.
t	thickness of shield, in.
ϵ	emissivity
ϵ_s	emissivity of shield

SHADOW SHIELDS OR THERMAL RADIATION shields provide an effective means of limiting heat transfer for many space vehicle applications. Studies in the area of thermal protection for solar probes (e.g., (1)* and (2)) and for cryogenic propellant tanks (e.g., (3)) have indicated that substantial weight savings can be obtained with the use of shadow shields.

The shields are best applied on long-term interplanetary missions where the space vehicle can be sun-oriented. (The orientation requirement does not appear to be a detriment since most lunar and planetary spacecraft to date have utilized sun orientation.) In Earth orbital missions or missions in the near vicinity of other planets, fixed-shadow-shield systems cannot effectively be used to simultaneously afford thermal protection from both the sun and the planet and, hence, must be augmented by other insulation systems.

Shadow shields with varying shapes have been analytically investigated (4, 5, 6, 7, 8) including flat plates, spheres, hemispheres, cones, etc., and combinations thereof. Very little experimental effort has been made in this area other than that on a single flat shield for solar-probe temperature control (9) and on inflatable balloon shields for cryogenic storage (5). The work presented herein examines the thermal characteristics of multiple flat shields--both ideal and practical. One advantage of the flat shields is that they will take up little space on a vehicle and can be used internally (e.g., between a cryogenic tank and a payload). The experimental program was undertaken to: (1) verify existing analysis for predicting shield performance, (2) extend our analytic capabilities for predicting the performance of more realistic systems, and (3) provide an insight to some of the practical problems involved with a shadow-shield system.

Experimental data were obtained on the effect of shield spacing, number, surface properties, and lateral conduction on the overall shield performance. A scale model of a shadow-shield system was also designed, fabricated, and tested to examine some of the more practical problems of shield application.

EXPERIMENTAL APPARATUS

The experimental apparatus consisted of a vacuum chamber, a temperature-controlled heat source, a liquid-nitrogen tank heat sink, and the necessary instruments to record temperatures and heat-transfer rates.

The heat-transfer experiments were performed in a vacuum chamber to eliminate gaseous conduction. The chamber consisted of a cylindrical section 5 feet in diameter and 6 feet in length with two elliptical end covers. One end cover was mounted on a movable dolly to provide easy access to the chamber. The cylindrical section contained a 4-foot diameter liquid-nitrogen-cooled shroud maintained at about 140° R. Liquid nitrogen shrouds for the end covers were mounted on the movable end cover. With the liquid-nitrogen-cooled walls, the chamber was capable of operating continuously in the 10^{-7} to 10^{-8} Torr range.

The heat source, heat sink, and shadow-shield configuration were all mounted on the movable end cover as shown in figure 1. (Note the two liquid nitrogen shrouds for the end covers that were discussed previously.) The heat source consisted of a 1-inch-thick copper disk, 12.75 inches in diameter, with calrod heaters on one side and a surface coated with a high temperature paint (about 2 mils thick) on the other side. The paint was capable of retaining its known thermal properties during continuous operation at temperatures up to 810° R. The heater was mounted above a stainless steel framework which was, in turn, suspended by low-conducting stainless steel cable.

The heat sink consisted of a copper liquid nitrogen tank suspended by four stainless steel rods. (Its diameter was also 12.75 in. as were all shields and tanks tested.) Considerable effort was made to minimize the amount of heat conducted into the tank by the supports and fill and vent lines. The stainless steel beams supporting the entire experiment were cooled with LN_2 for this purpose. The bottom of the tank was painted with a high-emissivity paint as was the entire liquid nitrogen shroud for the vacuum chamber. The paint's absorptivity or emissivity was about 0.86 at 140° R.

The cage structure surrounding the LN_2 tank was used to suspend the shields and heater and to provide a means of varying the shield spacing during an experimental run. By use of a series of pulleys, cables, and an external crank, the scissors mechanism shown could be adjusted for heater distances up to 12 inches. The purpose of the scissors mechanism was to maintain equal spacing between the shields for any heater setting. Again, the shields were supported by low-conducting cable and, in some cases, by fine locket chain.

Figure 2 shows an aluminum tank with a $\sqrt{2}$ elliptical bottom mounted in place for testing. This tank and its attached scale-model shadow-shield configuration (fig. 3) was used for practical shield tests as will be discussed later.

The measuring and recording equipment consisted of wet test meters to record the boiloff from the LN_2 tank, temperature recorders, and vacuum gages. The boiloff rate or volume flow rate from the LN_2 tank was used to determine the heat-transfer rate. Thermocouples were used to determine the temperatures of the heater, shields, and LN_2 tank as well as the temperature of the solid conduction paths into the LN_2 tank (i.e., support rods, fill lines, and vent lines). Considerable care was exercised in thermocoupling the shadow shields in order to avoid disturbing the shield temperature profile. For example, the thermocouple leads (3-mil diameter) for the thinner lightweight shields were laid along isotherms for some distance before leaving the shield to eliminate any influence of the lead wires. The vacuum gages were monitored to insure that the

*Numbers in parentheses designate references at end of paper.

vacuum chamber pressure remained below 10^{-6} Torr where the gaseous conduction was negligible.

PROCEDURE

In a typical experimental run, the apparatus was cold-soaked for 4 to 5 hours to ensure that all the lines and support rods leading to the LN_2 tank were sufficiently cooled to minimize conductive heat inputs. Then power was applied to the heater to maintain it at a given temperature ($\pm 1^\circ$) until the boiloff rate and all shield temperatures stabilized. The boiloff gas from the LN_2 tank passed through a constant pressure device into a saturation pot and then through a wet test meter where the volume flow rate was determined. The constant pressure device isolated the LN_2 tank from fluctuations in the atmospheric pressure. The volume flow rate along with tank pressure and the wet-test meter temperature and pressure were used to determine the heat-transfer rate into the LN_2 tank. This heat-transfer rate less the calculated miscellaneous heat leaks (on the order of 1 to 2 Btu/hr) represented the net radiant heat-transfer rate into the bottom of the LN_2 tank. Shield, tank, and heater temperatures were determined by direct readout potentiometers or on recording potentiometers.

Subsequent data points were obtained by either varying the heater distance or temperature. Heater-to-tank spacings and their corresponding shield spacings were observed via a chamber porthole and a movable flap in the liquid nitrogen shroud. Heater temperatures of 520°, 650°, and 800° R were used with the majority of the data taken at 650° and 800° R. The higher temperatures were used to drive the heat-transfer rate up into a measurable range for the lower-heat-flux shield configurations.

ANALYTICAL AND EXPERIMENTAL RESULTS

SHIELD SPACING AND NUMBER - The radiant heat-transfer rate through a set of equal diameter shields depends upon the shield spacing, number, surface properties and lateral conductance, as well as the boundary temperatures. In order to investigate the effects of each of these variables, it is desirable to begin with the simplest case and systematically vary one variable at a time. The most readily analyzed case is that with infinitely conducting shields or shields that have no temperature gradients. An example of this is shown in figure 4 where the individual shield temperatures are shown as a function of spacing ratio for the five-shield configuration shown in figure 1. Spacing (L/R_o) is the total distance between the heater and tank divided by the common tank radius. The heater temperature was 800° R. The solid lines represent the analytical results for infinitely conducting shields.* The circles are data points for 0.0625-inch copper shields which closely represent infinitely conducting shields for the radius used. (The temperature gradient from the center of the shields to their outer edges varied from 2° to 4° for the experimental runs shown.) The shields were coated with the same high-temperature paint used on the heater. Its emissivity was temperature dependent and varied from 0.88 at 140° R to 0.983 at 800° R, with a room temperature value of about 0.94. This paint (designated $\epsilon_s \approx 0.94$ on the figures) was used throughout most of the experimental program to provide surfaces with consistent properties.

It is evident from this figure that the analytical and experimental temperatures are in close agreement. For the two spacings shown, 0.47 and 0.94 (3 and 6 in. between heater and tank), the maximum deviation between the analytical and experimental temperatures is $\pm 6^\circ$ for any one of the five shields. The heat-transfer rates for this five-shield configuration as well as those for zero-, one-, and three-shield configurations are shown as a function of spacing ratio in figure 5. The heater temperature used was 800° R. Here too, the agreement between the analysis (solid line) and experimental data (circles) is good--on the order of ± 5 percent for most of the data points shown. The advantage of using shields to reduce radiant heat transfer is quite apparent. For example, the heat-transfer rate with no shields, for a distance of 1 inch between the heater and tank ($L/R_o = 0.157$), is 506 Btu per hour per square foot. Inserting one shield in the 1-inch space reduces the rate to 263 Btu per hour per square foot. Furthermore, the relative advantage of shields is minimized here because of the high-emissivity surfaces used (high emissivities gave relatively high heat-transfer rates which allowed more accurate measurements). In an actual application, lower emissivities would be used and would further enhance the relative gains to be made.

SHIELD EMISSIVITY - The effect of shield emissivity on heat-transfer rate is demonstrated in figure 6 for one and three shadow shields, respectively. Again, an 800° R heater temperature was used. The upper two curves are for one and three painted shields ($\epsilon \approx 0.94$) as shown in figure 5. The lower two curves are for 0.0625-inch-thick copper shields that have been glass-blasted to provide a clean, uniform surface ($\epsilon \approx 0.27$). Hence, the only variable changed was surface emissivity. The emissivity of both surfaces varied with temperature and was accounted for in the analysis although only the room temperature values are noted. The dotted and solid lines represent the analytical results for one and three infinitely-conducting shields, respectively. The circle and triangle symbols represent the corresponding experimental data. Again there is close agreement with the analysis with the exception of the three-shield, low-emissivity point at a spacing of 0.63. The measured heat-transfer rates at these levels lose some accuracy due to the uncertainty of calculating the miscellaneous system heat leaks

*Results from IBM 7094 computer program which utilizes equations from reference 4 modified to include variable emissivities for the individual shields.

(through plumbing, instrumentation leads, etc.) which are on the order of 1 to 2 Btu per hour. Despite this, the overall agreement is good and clearly indicates the strong effect of shield emissivity on the heat-transfer rates. The potential advantage of shadow shields start to become evident here. For example, by inserting three clean copper shields ($\epsilon \approx 0.27$) in a 1-inch gap between the 12.75-inch diameter heater and tank, the heat flux can be reduced from 506 to 17 Btu per hour per square foot, a factor of 30. If aluminum shields ($\epsilon \approx 0.03$) were used for this same configuration, the calculated heat flux would be on the order of 0.12 Btu per hour per square foot, a four thousandfold reduction.

SHIELD LATERAL CONDUCTION - Since thick copper shields are impractical for most applications due to weight considerations, it is desirable to know the effect of using thinner, lighter materials. The analysis for conducting and nonconducting shields is somewhat complex and for purposes of simplicity is not presented here. Briefly, the same general calculation techniques given in references 4 and 6 were used with changes to include the effect of conduction. Each shield was broken up into a series of annular rings and a heat balance was performed on each individual ring. If the shield is assumed to be nonconducting, the only way heat can reach the ring is by radiation and reflection from sources which are in a position to see the ring (other rings, heater, etc.). If the shield is assumed to be conducting, additional heat can enter or leave the ring by solid conduction from adjacent rings. Since numerical integration was necessary, the equations were programed on an IBM 7094 computer. The results of this computer program are used throughout the remainder of the paper.

Figure 7 demonstrates the effect of lateral conductance on shield temperature profile for a single shield centrally located between a heater and tank 2 inches apart. The heater temperature is 650° R. Three separate shields, all coated with the high-temperature paint, were used; 0.0625-inch copper, 0.015-inch stainless steel, and 0.002-inch Mylar. The value of kt/R_o (thermal conductivity times thickness over radius) which determines the shield temperature profile is given for all three shields. The abscissa represents the position on the shield radius; zero for the shield center, and one for the outside edge of the shield. The solid lines represent the analytical predictions and the symbols the experimental data. Although the experimental temperatures are displaced a few degrees, the agreement with theory is quite good, especially the general shape of the temperature profile.

Note the large temperature gradient across the low-conducting Mylar shield--on the order of 80° R. This large gradient results because the lateral conduction is low, leaving only the radiation heat transfer to determine the temperature profile. Since surface emissivities are high, the center of the shield absorbs more heat from the heater due to the relatively high view factor from the heater to the shield center. This is further demonstrated in the three-shield system shown in figure 8 where each shield is exposed to one or two surfaces that are nonuniform in temperature. The relative spacing between the painted shields is the same as in figure 7, although a higher heater temperature was used. The temperature at the center of the middle shield is about the same as the heater temperature used for figure 7. The outer edges, however, are much cooler which, in turn, allows the outer edges of the colder shield to decrease further. The temperature gradient across this shield is on the order of 140° R. The analytical (solid lines) and experimental temperatures (symbols) as well as the heat-transfer rates are in close agreement.

The effect of shield temperature gradients on the heat-transfer rate is shown in figure 9 where the ratio of kt/R_o is varied for the three-shield system. The three Mylar shields used for figure 8 have a kt/R_o ratio of 2×10^{-5} Btu per hour per foot per °R. Data points are also shown for stainless steel, aluminum, and copper shields. The agreement between analytical and experimental results is close and indicates that the zero conducting shields will have a heat-transfer rate approximately 20 percent higher than infinitely conducting shields. This difference will vary depending on the number of shields, emissivity, and spacing. However, it appears that the simpler infinite-k analysis (4) could suffice for rough estimates of shield heat-transfer rates.

SHIELD TARGETING - Since space-vehicle weight considerations will probably dictate the use of thin shields or low-conduction shields, the temperature profiles across shields must be considered in the system design. For some applications, it may be of interest to alter the shield temperature profile. This can be accomplished by selectively coating various annular rings (targeting) on a shield or shields. An example of how a shield temperature profile can be altered is given in figure 10 for a two-shield configuration. All the shield surfaces are again painted with the high-temperature paint with the exception of a shiny aluminum disk (see sketch on fig. 10) on the shield next to the heater. The material used for this shield was aluminum-Mylar-aluminum laminate (AMA-0.00035 Al, 0.001 Mylar, and 0.00035 Al). Without targeting, the shield temperatures would be warmest in the center and decrease monotonically outward as they did in figures 7 and 8. The effect of targeting is quite pronounced as is evidenced by the sharp temperature increase near the edge of the colder shield. Despite the large temperature excursion, the analysis adequately predicted the results. The particular targeted system used here has little practical value and was designed primarily to determine if the analysis* could sufficiently predict the re-

*It is planned to publish the analysis in a future report.

sults. In a more realistic application, the shield temperature profile might be altered for thermal stress considerations or to lower the net heat-transfer rate through a shield system (preliminary calculations indicate that a 10-or 20-percent reduction is feasible for long-term cryogenic storage).

PRACTICAL SHADOW-SHIELD SYSTEMS - The results thus far have considered only shields that are thermally isolated; that is, shields that have no conduction to or from the shield. For this reason, thin wire and locket chains were used to suspend the experimental shields. In a practical application, a structural system will be required to support the shields in their proper positions so it becomes necessary then to determine the effect of the struts on the shadow-shield performance.

The approach taken in the experimental program was to design a shadow-shield system for a hypothetical cryogenic stage, scale it down, and test it. The vehicle considered was a 7000-pound hydrogen-oxygen stage capable of delivering a payload to a Mars orbit. Trip time was 200 days during which time the vehicle was sun-oriented with the payload toward the sun. Two shields were located in a 12-inch gap between the liquid hydrogen tank and the payload with the first shield 1.5 inches and the second 10 inches from the hydrogen-tank surface. (Preliminary analysis of the two-shield configuration indicated that the radiant heat transfer could be minimized by placing one shield near the tank and the other near the payload.) Tank and payload diameters were 10 feet. One-half inch was allowed for ground-hold insulation (3) which could consist of foam insulation with a few external layers of double-aluminized Mylar. The double-aluminized Mylar could afford protection during near-planetary operations. The shadow-shield system selected was not optimized, but was capable of limiting the hydrogen-tank radiant-heat input from a 530° R payload to about 0.22 Btu per hour. From a radiation standpoint alone, this results in 5.5 pounds of hydrogen boiloff for the entire mission. It is estimated that the entire shield system would weigh roughly 90 pounds* including about 50 pounds for ground-hold insulation. The heat-transfer rate through the structural support system separating the tank and payload was on the order of 2 to 3 Btu per hour indicating a total heat leak on the order of 3 Btu per hour (or about 75 lbs boiloff for the mission). The magnitude of these heat leaks indicates that efforts to reduce the overall heat leak should be concentrated in the area of the support system.

*If a typical multifoil insulation or "superinsulation" system were used to protect the hydrogen tank, rather than the shadow shields, about 150 lb of insulation would be needed resulting in a mission boiloff of 150 lb. (Assumed 5 lb/ft^3 insulation with a temperature-dependent thermal conductivity--room temperature value = 5×10^{-4} (Btu)(in.)/(hr)(ft^2)(°R)).

A scale model of the system is shown in figure 2 with details of the shield design shown in figure 3. The scaled-down model used for testing was the result of several compromises to facilitate testing in the environmental chamber. The tank, payload, strut and shield ring dimensions, and shield spacings were all linearly scaled down from the full-size version making the radiation exchange between components equivalent. The cross-sectional area of the struts and shield rings (fig. 3), however, were determined primarily by the availability of existing materials and as a result were not scaled properly. The struts were 0.1-inch diameter, 0.012-inch wall stainless steel tubes. The 12.75-inch shield rings, upon which the double-aluminized Mylar was cemented, were 0.125 inch in diameter with 0.01-inch walls. The shield material used, 1/4-mil double-aluminized Mylar, is, for all practical purposes, nonconducting and is representative of the full-scale shield material. The struts were brazed to the 0.25-inch copper plate (fig. 3) to insure good thermal contact with the simulated payload. The opposite ends of the struts were brazed to copper pads (fig. 2) which were, in turn, forced against the tank by a stainless steel band. This arrangement allowed the flexibility of changing the shields or shield configuration. In order to provide surfaces with known emissivities, both the tank and simulated payload were coated with the same paint used on the tank and heater in the previous tests. Normally, these surfaces would be reflecting surfaces with low emissivities. Finally, liquid nitrogen, rather than liquid hydrogen, was used for safety reasons. Despite these departures from the full-scale system, the model was sufficient for probing into some of the strut-shield interactions of realistic systems.

The temperature profiles that the shields would assume independent of the struts are shown in figure 11(a). The shields were suspended between the ellipsoidal LN_2 tank and a 650° R heater by fine locket chain. The solid line on the figure represents the analysis and the circle symbols, the experimental data. The dark circles give the measured temperature of the colder shields. (Throughout the remainder of this paper, the shield nearest the tank will be referred to as the colder shield and that nearest the simulated payload will be referred to as the warmer shield.) The edge temperature ($R/R_o \approx 1$) of the warmer shield drops off sharply because of the relatively high-emissivity ($\epsilon = 0.3$) stainless steel rim which acts as a target (see fig. 3). Likewise, the edge of the colder shield increases in temperature because the exposed side of the ring faces the exposed side of the warmer shield ring. The shield emissivity was difficult to determine, but it is estimated that it is between 0.023 and 0.035. A constant value of 0.03 was assumed. The agreement here is not as good as on the previous figures for several reasons: (1) the exact emissivities of the highly-reflective shields and the stainless steel rims are not known, (2) the analysis considers flat shields only and does

not account for the rings, and (3) the technique used to apply the thermocouples to the thin shield altered the shield temperature somewhat. Despite this, however, much can be gained from the data as will be demonstrated.

Figure 11(b) gives a rough estimate of the strut temperature profile between the simulated payload (650° R at zero distance) and the LN_2 tank. The profile assumes there is no physical contact between the strut and shield and considers only conduction down the strut and radiation from its surface. The symbols are experimental temperatures for shields pinned in place with stainless steel pins. The location of the shadow-shield rims are denoted by the dashed lines. Note how much lower the rim temperatures are (fig. 11(a)) compared to the strut temperatures at the corresponding positions. Since the major portion of heat transfer through the shadow-shield system is via the supports, it would appear beneficial to solidly join the strut and shield rim. In this way, the shield rims could act as fins to help lower the strut temperatures which would, in turn, lower the net heat reaching the cryogenic tank. Only a small fraction of the heat radiated from the warmer shield rims would reach the tank.

Figures 12(a) and (b) depict the shield and strut temperature profiles with the shadow shields welded into the structural cage. The same analytical profiles given in figure 11 are presented here for reference. The weldments for the two shields are 0.48 and 0.74 inch from the 650° R simulated payload as shown in figure 3. Comparing the experimental data on figures 11 and 12, note how the shield rim temperatures have increased and how the strut temperatures have decreased for the welded system. Based on a simple comparison of the experimental strut temperature-drops (295-155/320-155), the heat transfer through the welded system will be reduced to 0.85 of that through the nonwelded (pinned) system. Similarly, the radiant heat transfer will be 1.5 times higher ($\overline{360}^4/\overline{310}^4$) for the welded system due to the higher shield temperature. The net heat-transfer rate, however, will be lower because the larger portion of the heat is transferred through the structural members (for the cryogenic stage used, about 90 percent of the heat transfer was due to the struts).

EFFECT OF STRUT EMISSIVITY - Another means of lowering the strut temperature profile can be accomplished by selectively coating the struts with a high-emissivity material to help radiate some of the heat away. The results of an experiment to determine the effect of strut emissivity are shown in figure 13. Two 12-inch, 5/8-inch outside diameter by 0.035-inch wall stainless steel struts were connected between a 800° R heater and the flat-bottomed LN_2 tank. The two shields were inserted between the heater and tank to make the radiation heat transfer negligible. The temperature profiles are shown for clean stainless steel struts ($\epsilon = 0.3$) and partially coated struts ($\epsilon = 0.6$). The partially coated struts denoted by the dashed line and the triangle symbols consisted of a clean strut with the outer half coated with the high-temperature paint as shown in the sketch. This maximized the heat that could be radiated from the strut and minimized the heat transfer on the side facing the heater. The simplified analytical model used (same as used on figs. 11 and 12), however, did not distinguish between the high- and low-emissivity areas but rather assumed an average emissivity. It also did not include the effect of radiation from the heater and shields or internal strut radiation. Although the absolute agreement between the rough analysis (solid and dashed lines) and experimental data (symbols) is poor, the magnitude of the relative effect of the coating is in good agreement. Inaccuracies in calculating miscellaneous system heat leaks, on the order of 1 to 2 Btu per hour, seriously compromised the accuracies of the measured heat fluxes. However, it is evident that coating the struts measurably lowers the heat-transfer rate.

Coatings were applied to both the struts and the outer edges of the shield rings of the practical system in an effort to further lower the strut temperatures. The results are given in figure 14. The shield rims were targeted as shown on the sketch. Because of the small size of the experimental model, the entire circumference of the strut was coated rather than just the outer half. Again, the payload temperature was held at 650° R. The analytical profiles given are the same as given on figures 11 and 12 and are used only as points of reference. No attempt was made to formulate an analytical model for the integrated system.

It is apparent from the figure that the applied coatings signficantly lowered the strut temperature. For example, at a distance of 4.3 inches from the payload, the temperature dropped from 295° R on the uncoated system (fig. 12) to 260° R on the coated system. This means the strut heat transfer through the coated system will be reduced to 260-155/295-155 or 0.75 of that for the noncoated system. The radiation from the shield will increase slightly due to the targeted edge, but the overall heat-transfer rate of the combined system will be reduced measurably by coating the struts and shield rims.

DOUBLE-SHEETED SHIELDS - As mentioned previously, the shadow-shield system selected for the practical system was not necessarily optimized. Improvements in performance could be obtained by adding more shields, increasing the spacing, improving the shield surface properties (e.g., using gold rather than aluminum deposits on the Mylar), or possibly targeting as indicated in the former figures. Another method of improving the shield performance can be realized by adding an extra shield to each shield support ring as shown in the sketch in figure 15. Here, a sheet of 0.00025-inch double-aluminized Mylar is cemented to each side of the ring, completely enclosing the ring. The temperature profiles of the double-sheeted shields are given for the same spacing and simulated

payload temperatures as used in the single-sheeted shield tests shown on figure 11(a). Note how the experimental temperature of the shield facing the LN_2 tank decreases from 310° R for the single-sheeted shield (fig. 11(a)) to 210° R for the double-sheeted shield. This represents about a factor of 4.7 decrease in the radiant heat-transfer rate. The corresponding analytical temperatures indicate a factor of 4 decrease and are probably more representative of the reduction because of the inaccuracies in measuring shield temperatures. In addition to the improved shield performance, the lower rim temperature on the colder double-sheeted shield could also help reduce strut losses as pointed out previously.

The analysis (solid lines) for the double-sheeted shields is the same as that used throughout the paper. Because the analysis only considers flat shields, the spacing between the double sheets was assumed to be very small to force the view factors to approach one. This is not an unreasonable assumption since no radiation can escape from between the sheets. The agreement between the analysis and experimental data is fair with the exception of the rim temperatures which cannot be predicted accurately due to the presence of the ring.

The double-sheeted shield concept applied to the full-scale cryogenic stage would limit the radiation heat-transfer rate from the shields to the liquid hydrogen tank to about 0.05 Btu per hour or 1 to 2 pounds boiloff for the mission discussed previously. This is a factor of 4 less than that from the single-sheeted concept. Because of the improved efficiency of the double-sheeted shields, the distance between the payload and hydrogen tank (11.5 in.) could be further decreased to make a more compact system.

CONCLUDING REMARKS

Summarizing, the effects of various basic parameters on shadow shield performance were investigated including number of shields, spacing, emissivity, and lateral conductance. The results were as follows:

1. Experiments performed on 0.0625-inch-thick copper shields verified the infinitely conducting shield analysis presented in reference 4. The predicted results were, in general, within ±5 percent of the experimental data.

2. The in-house analysis developed for conducting and nonconducting shields accurately predicted the experimental data. Both analytical and experimental results demonstrated that large temperature gradients can be encountered in the more practical low-conducting shields. Despite these temperature gradients, the heat flux can generally be predicted within 20 percent by the simplified infinitely conducting shield analysis.

3. Experimental results also verified the analysis developed for targeted shields. Targeting or varying the surface emissivity of annular rings can be used to alter the shield temperature profile, or, in some cases, to lower the overall heat-transfer rate.

Tests on a scale model of a practical shadow-shield system for cryogenic storage revealed the following:

1. The use of a peripheral ring with a light shield material stretched over it is a practical lightweight method of constructing a shadow shield.

2. The integration of a shield system and its support system does not necessarily cause a deterioration in overall system performance. Providing a good thermal contact between the shield edges and their supporting structure can actually enhance the overall performance in some situations. In general, this will occur only when the shield rim temperatures are lower than the strut temperatures at the junction point.

3. The heat transferred through structural members connecting warmer components with a cryogenic tank can be reduced significantly by selectively coating the structural members with a high-emissivity material. Where shields are solidly connected to structural members, coating the shield rings (or targeting) can also help reduce strut heat transfer.

4. Double-sheeted shields, consisting of a peripheral ring with shield material stretched over both sides far outperforms single-sheeted shields with little addition in shield weight. From the experimental data, it appears that the existing analyses can adequately predict the shield temperature profiles with the exception of the rim temperatures which were not included in the analysis.

Both the experimental and analytical results demonstrate the potential of shadow shields as a method of thermal control. The scale-model tests demonstrated a feasible method of lightweight shield construction and that the shields could be packaged in a relatively small space between vehicle components. There are, no doubt, many more methods of constructing lightweight shields (e.g., inflatable shields) and methods of attachment. Further work could be done in this area. The analysis developed, adequately predicts shield performance and can be used to determine how and where the shields should be attached to their supporting structure. The interaction between thermally-bonded shield rings and struts was not considered analytically, however, so additional work could also be done in this area.

Although the analytical and experimental work concentrated primarily on shadow shields applied between an on-board heat source and a cryogenic tank, many other shield applications exist. Shadow shields could also be used to protect a cryogenic propellant tank from solar heating or to protect a solar-probe payload from intense solar heating during near passes to the sun. For long-term storage of cryogenics, shadow shields will provide an efficient method of reducing the boiloff rates (venting rates) of cryogenic propellant tanks. Shadow shields will also take on added importance for missions where the number of propellant-tank venting cycles must be minimized.

REFERENCES

1. Lundholm, J. G., Jr.; Prohaska, E. S.; Hoyer, S.; and Averell, J.: A Close Approach Solar Probe Design Feasibility and Mission Study. Paper No. 64-496, AIAA, June 1964.

2. Hall, Charles F.; Nothwang, George J.; and Hornby, Harold: Solar Probes - A Feasibility Study. Aerospace Eng., vol. 21, no. 5, May 1962, pp. 22-30.

3. Knoll, Richard H.; and Oglebay, Jon C.: Lightweight Thermal Protection Systems for Space Vehicle Propellant Tanks. Paper No. 746C, SAE, Sept. 1963.

4. Smolak, George R.; Knoll, Richard H.; and Wallner, Lewis E.: Analysis of Thermal-Protection Systems for Space-Vehicle Cryogenic-Propellant Tanks. NASA TR R-130, 1962.

5. Jones, L. R.; and Barry, D. G.: Lightweight Inflatable Shadow Shields for Cryogenic Space Vehicles. J. Spacecraft and Rockets, vol. 3, no. 5, May 1966, pp. 722-728.

6. Nichols, Lester D.: Effect of Shield Position and Absorptivity on Temperature Distribution of a Body Shielded From Solar Radiation in Space. NASA TN D-578, 1961.

7. Nothwang, George J.; Arvesen, John C.; and Hamaker, Frank M.: Analysis of Solar-Radiation Shields for Temperature Control of Space Vehicles Subjected to Large Changes in Solar Energy. NASA TN D-1209, 1962.

8. Arvesen, John C.; and Hamaker, Frank M.: Effectiveness of Radiation Shields for Thermal Control of Vehicles on the Sunlit Side of the Moon. NASA TN D-2130, 1964.

9. Arvesen, John C.: Effectiveness of Solar Radiation Shields for Thermal Control of Space Vehicles Subjected to Large Changes in Solar Energy. Symposium on Thermal Radiation of Solids. NASA SP-55 (AFML-TDR-64-159), 1965, pp. 549-557.

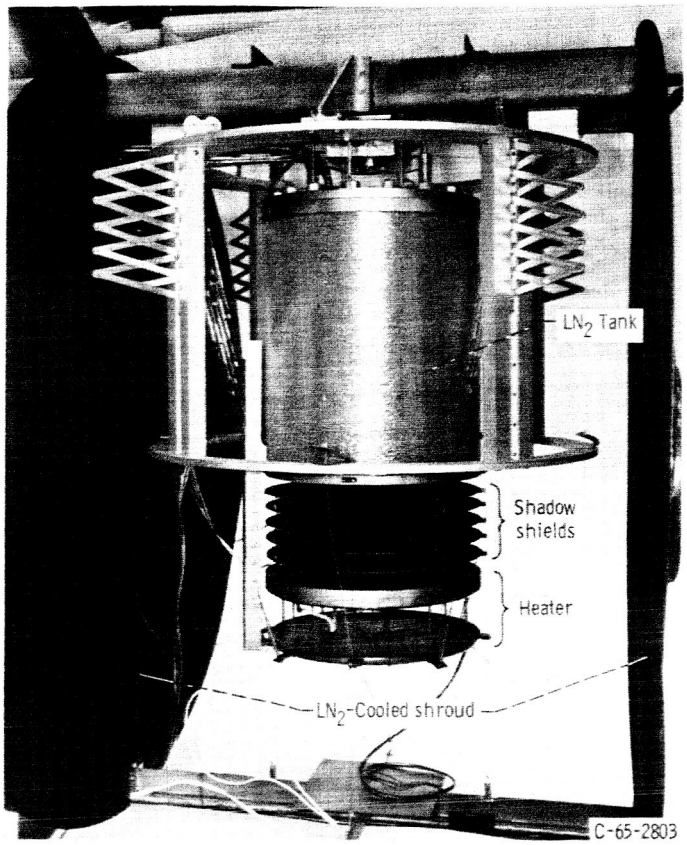

Figure 1. - View of five-shield configuration.

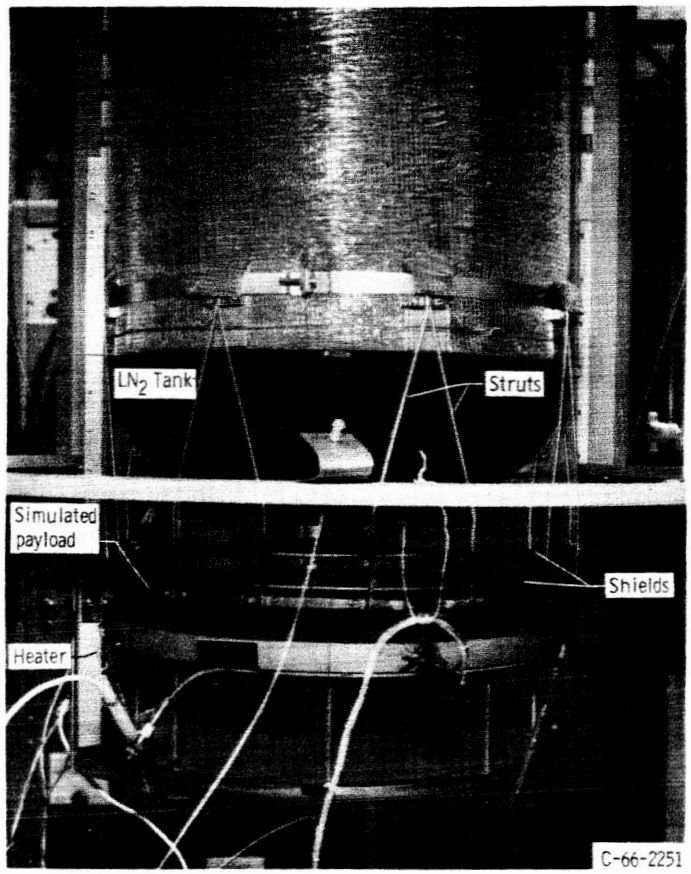

Figure 2. - Elliptical tank with scale-model shadow-shield system.

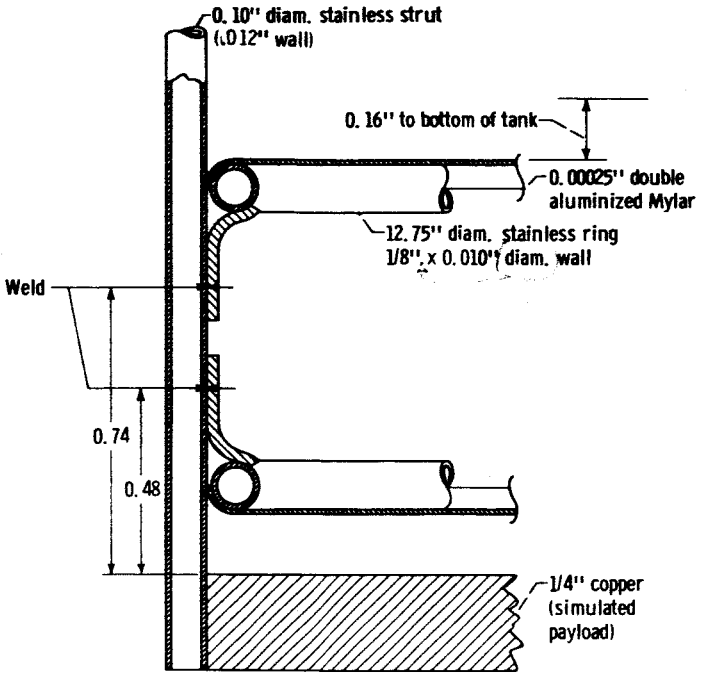

Figure 3. - Shield construction and method of mounting in practical system.

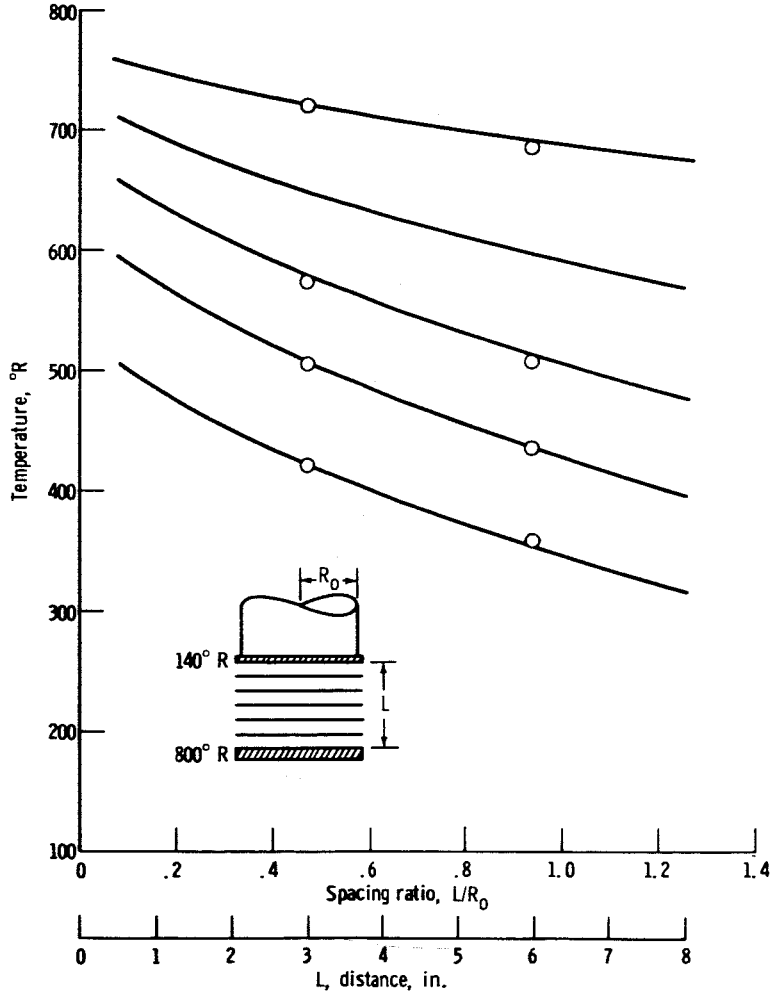

Figure 4. - Shield temperatures for five-shield system (ϵ_s = .94).

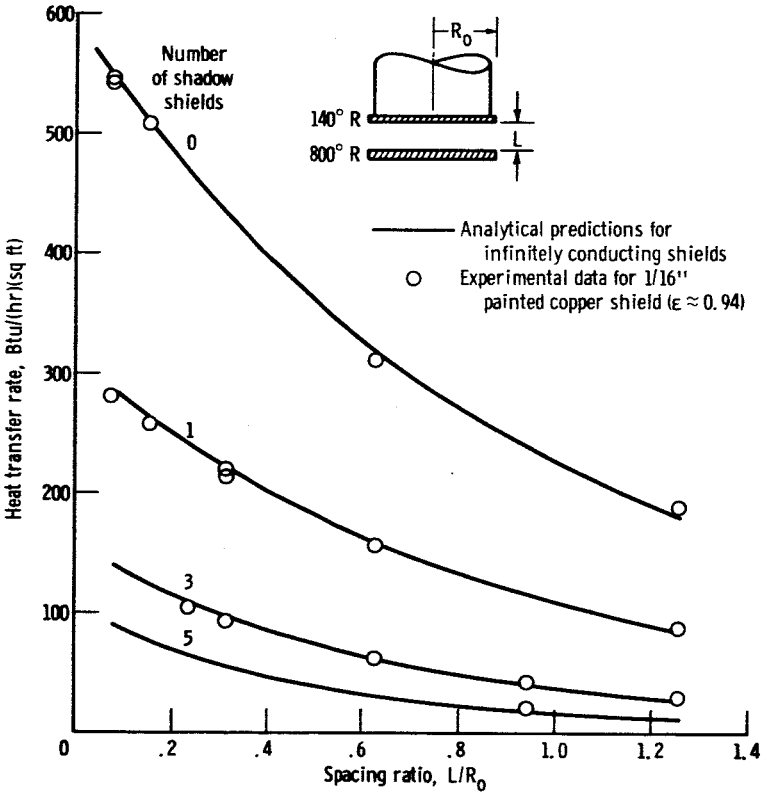

Figure 5. - Heat-transfer rate as a function of spacing and shield number.

E-3628

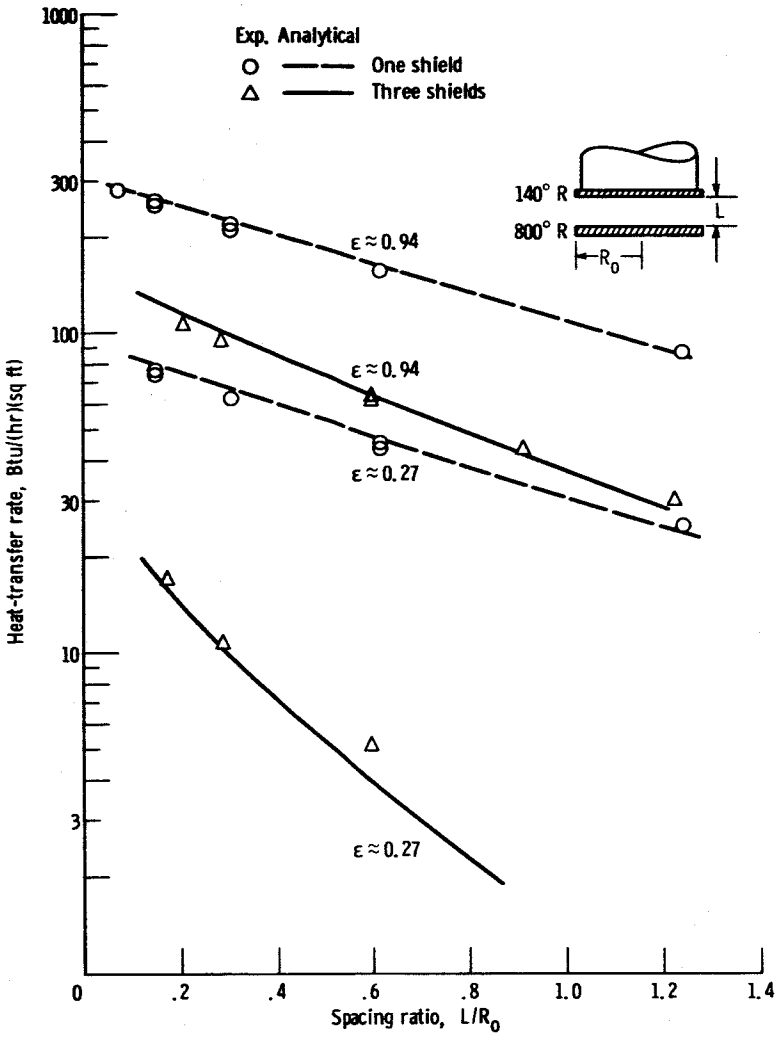

Figure 6. - Effect of shield emissivity on one and three shield systems.

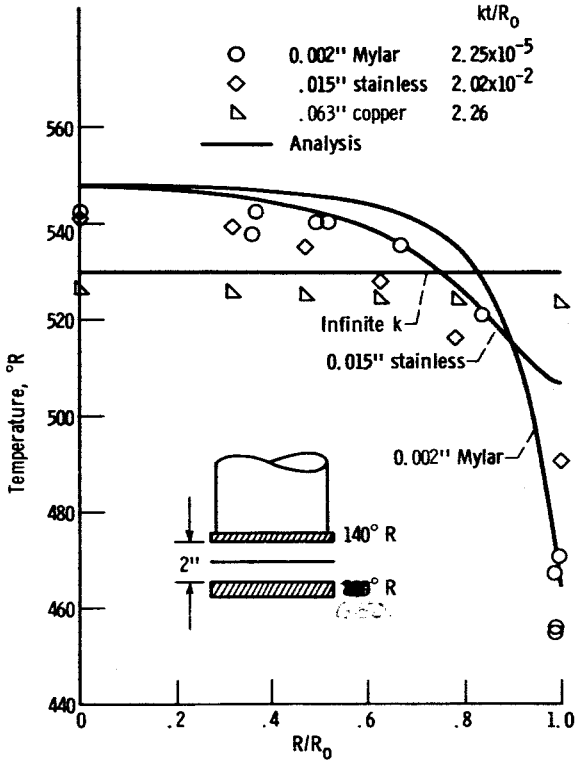

Figure 7. - Effect of lateral conduction on shield temperature profile (ϵ_s = .94).

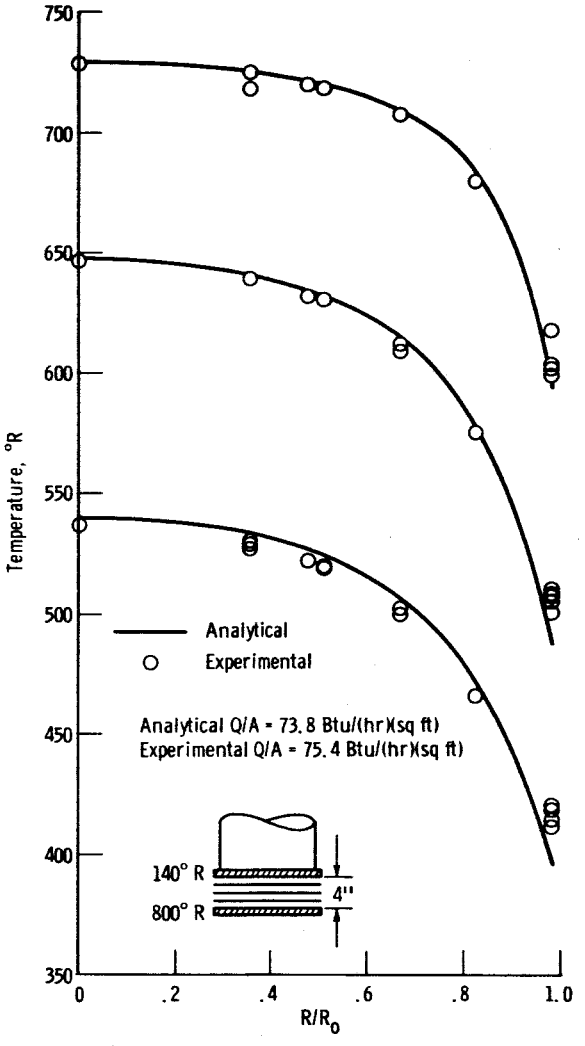

Figure 8. - Temperature profiles of three Mylar shields (ϵ_s = .94).

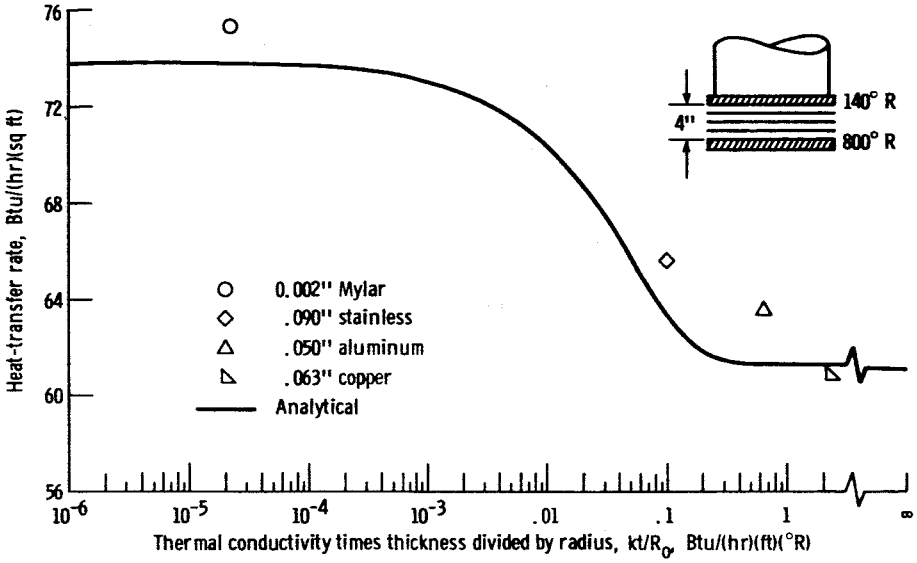

Figure 9. - Effect of radial conductance on heat-transfer rate for three shields (ϵ_S = .94).

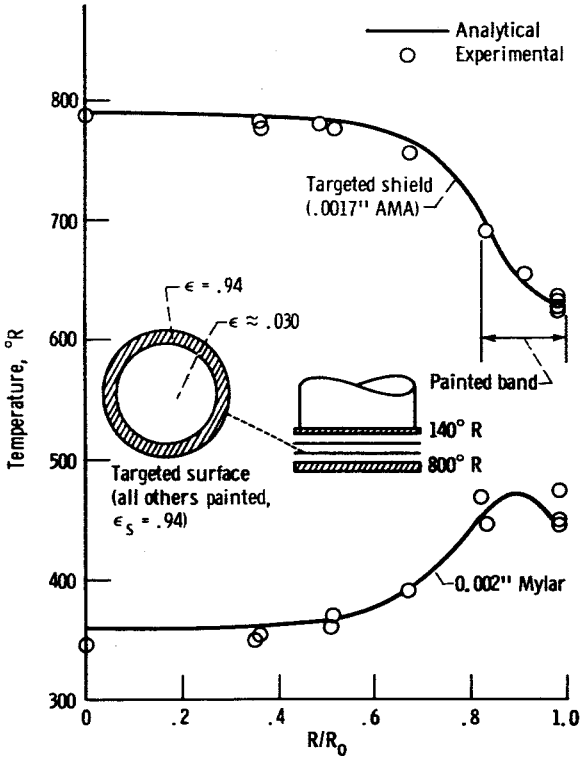

Figure 10. - Temperature profiles for targeted shadow shields.

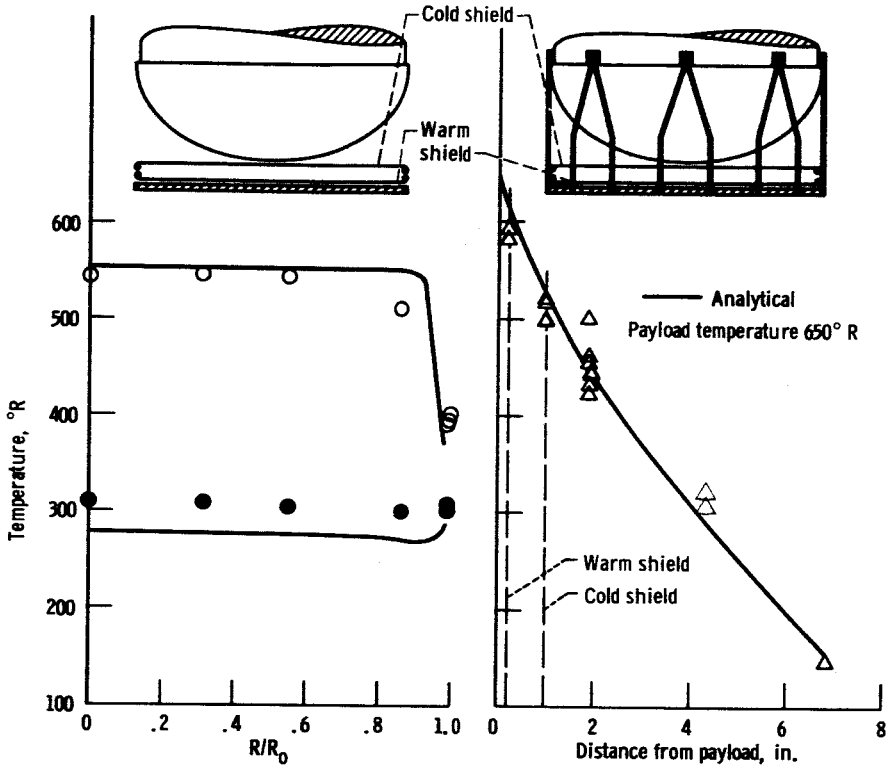

(a) Shield temperature profile.

(b) Strut temperature profile.

Figure 11. - Temperature profiles of shadow shields and support structure independent of each other.

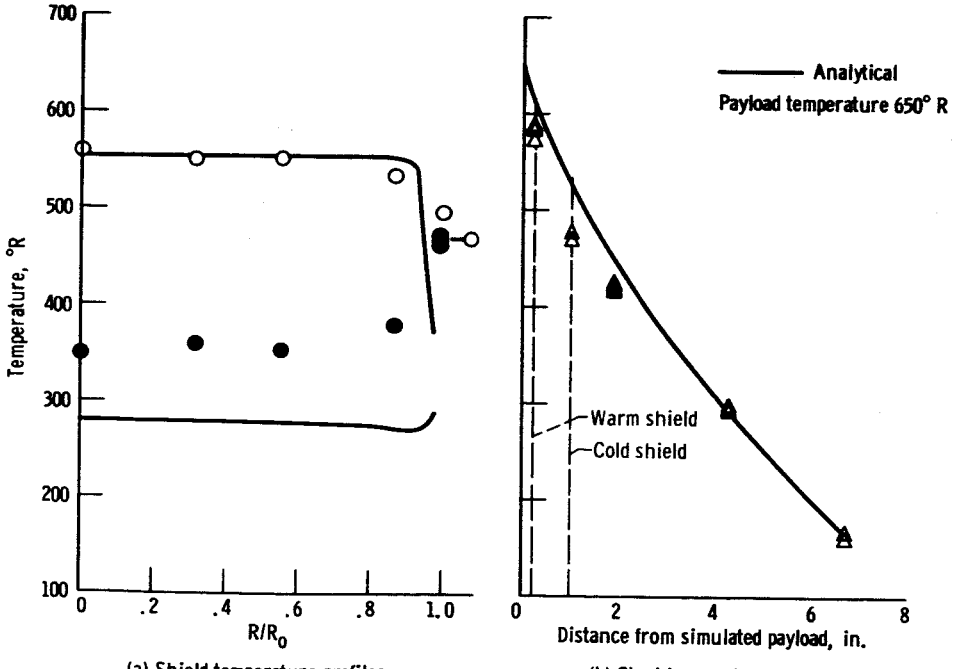

(a) Shield temperature profiles.

(b) Strut temperature profile.

Figure 12. - Temperature profiles with shields welded to support structure.

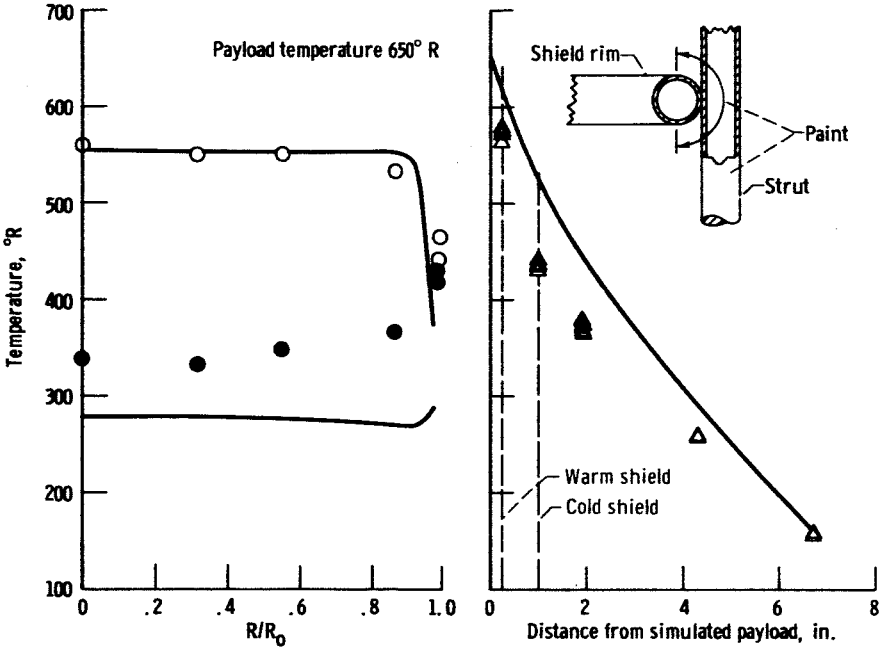

(a) Shield temperature profiles. (b) Strut temperature profile.

Figure 14. - Temperature profiles with shields and structure welded and targeted.

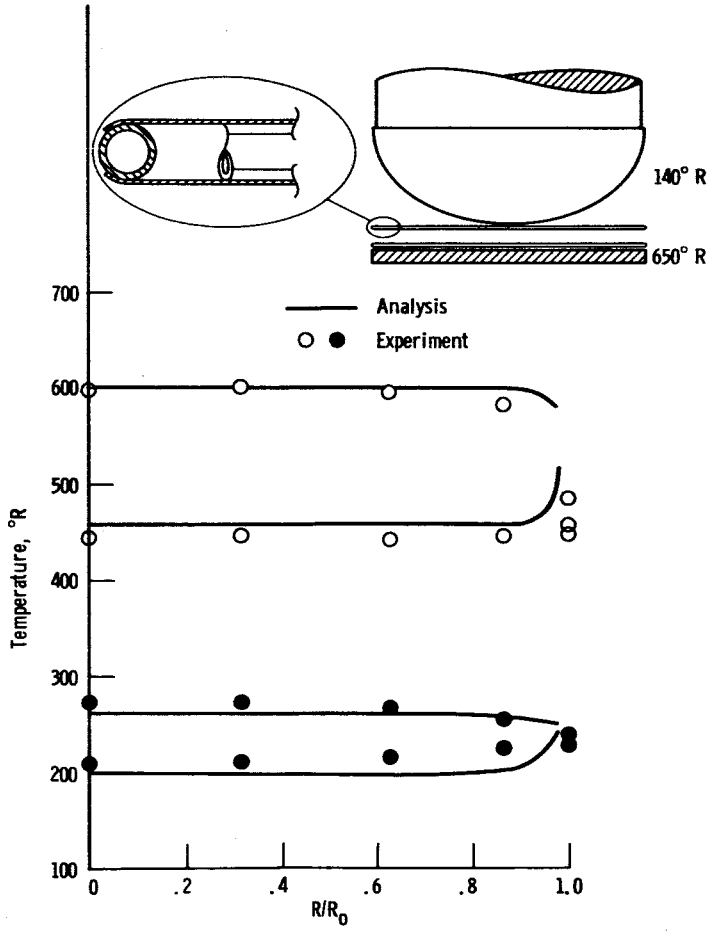

Figure 15. - Performance of double-sheeted shields.